



Ibuprofen biosorption by chemically activated *Saccharomyces cerevisiae*

ARTICLES doi:10.4136/ambi-agua.2862

Received: 07 Jun. 2022; Accepted: 02 Aug. 2022

Bruna Assis Paim dos Santos¹ ; **Evandro Luiz Dall'Oglio²** ;
Adriano Buzutti de Siqueira² ; **Danila Soares Caixeta^{1,3}** ;
Viviane Cristina Padilha Lopes¹ ; **Leonardo Gomes de Vasconcelos²** ;
Eduardo Beraldo de Moraes^{1,3*} 

¹Faculdade de Arquitetura, Engenharias e Tecnologias. Departamento de Engenharia Sanitária e Ambiental. Universidade Federal de Mato Grosso (UFMT), Campus Universitário de Cuiabá, Avenida Fernando Corrêa da Costa, n° 2367, CEP: 78060-900, Cuiabá, MT, Brazil. E-mail: bruna.santos_assis@hotmail.com, danilacaixeta@gmail.com, vivianelops@gmail.com

²Instituto de Ciências Exatas e da Terra. Departamento de Química. Fundação Universidade Federal de Mato Grosso (FUFMT), Campus Universitário de Cuiabá, Avenida Fernando Corrêa da Costa, n° 2367, CEP: 78060-900, Cuiabá, MT, Brazil. E-mail: dalloglio.evandro@gmail.com, buzutti7@hotmail.com, vasconceloslg@gmail.com

³Faculdade de Arquitetura, Engenharia e Tecnologia. Departamento de Engenharia Sanitária e Ambiental. Universidade Federal de Mato Grosso (UFMT), Campus Universitário de Cuiabá, Avenida Fernando Corrêa da Costa, n° 2367, CEP: 78060-900, Cuiabá, MT, Brazil. E-mail: danilacaixeta@gmail.com

*Corresponding author. E-mail: beraldo_morais@yahoo.com.br

ABSTRACT

Saccharomyces cerevisiae biomass was activated chemically, and its ibuprofen (IBP) biosorption capabilities were assessed regarding IBP removal from an aqueous solution. The effects of pH (2-10), contact time (0-90 min), IBP concentration (5-35 mg L⁻¹), and temperature (20, 30, 40°C) were evaluated in batch studies. Higher removal rates of IBP were found at pH 2.0. The pseudo-second-order kinetic model best described the experimental data. Both the Langmuir and Freundlich isotherm models described the equilibrium data satisfactorily. The maximum biosorption capacity for IBP onto chemically activated *Saccharomyces cerevisiae* biomass (CA-YB) was estimated at 13.39 mg g⁻¹ at 40°C. The activation energy calculated by the Dubinin-Radushkevich isotherm model was 9.129 kJ mol⁻¹, indicating that a chemical process mediated the biosorption of IBP onto CA-YB. According to thermodynamic studies, IBP biosorption is spontaneous and endothermic. FTIR analysis revealed that the carboxyl, hydroxyl, phosphoryl, and amino groups were involved in the biosorption process of IBP. These findings indicated that CA-YB could be an alternative biosorbent for IBP removal from aqueous media.

Keywords: isotherms, kinetic, microbial biomass, pharmaceutical drugs, thermodynamic study.

Biossorção de ibuprofeno por *Saccharomyces cerevisiae* ativada quimicamente

RESUMO

Biomassa de *Saccharomyces cerevisiae* foi ativada quimicamente e sua capacidade de



This is an Open Access article distributed under the terms of the Creative Commons Attribution License, which permits unrestricted use, distribution, and reproduction in any medium, provided the original work is properly cited.

bio sorção foi explorada para a remoção do ibuprofeno (IBP) da solução aquosa. Os efeitos do pH (2-10), tempo de contato (0-90 min), concentração de IBP (5-35 mg L⁻¹) e temperatura (20, 30, 40°C) foram avaliados em estudos de bateladas. Em pH 2,0 foram encontradas as maiores taxas de remoção de IBP. O modelo cinético de pseudo-segunda ordem foi o mais adequado para descrever os dados experimentais. Ambos os modelos de isoterma de Langmuir e Freundlich descreveram os dados de equilíbrio de forma satisfatória. A capacidade máxima de bio sorção para IBP pela biomassa de *Saccharomyces cerevisiae* quimicamente ativada (CA-YB) foi estimada em 13,39 mg g⁻¹ a 40°C. A energia de ativação calculada pelo modelo de isoterma de Dubinin-Radushkevich foi de 9,129 kJ mol⁻¹, indicando que um processo químico mediou a bio sorção de IBP por CA-YB. De acordo com os estudos termodinâmicos, a bio sorção do IBP é espontânea e endotérmica. A análise de FTIR revelou que os grupos carboxila, hidroxila, fosforila e amino estavam envolvidos no processo de bio sorção do IBP. Essas descobertas indicaram que CA-YB pode ser um bio sorvente alternativo para a remoção de IBP do meio aquoso.

Palavras-chave: biomassa microbiana, cinética, estudo termodinâmico, fármacos, isotermas.

1. INTRODUCTION

Widespread use of anti-inflammatory drugs is the main reason they are commonly detected in sewage wastewaters, surface and ground waters, and even drinking waters (Yamkelani *et al.*, 2019). During medical care, these drugs are excreted as unchanged or metabolites by animals and humans, and their concentrations in aquatic media are usually in the range of ng L⁻¹ or µg L⁻¹. Despite the low concentration, there is still cause for concern, as these pollutants are persistent, bioaccumulative, and endocrine disruptor (Oba *et al.*, 2021).

Ibuprofen [2-(4-isobutylphenyl) propanoic acid] is a non-steroidal anti-inflammatory widely used worldwide (Santaeufemia *et al.*, 2018). It is usually prescribed to relieve aches, pains, and fever. The concentration of ibuprofen (IBP) in the aquatic environment was found to range from 4198.4 to 10864.0 ng L⁻¹ in sewage wastewater, 5.7 to 223.6 ng L⁻¹ in drinking water, and 5 to 62 ng L⁻¹ in surface water (Aristizabal-Ciro *et al.*, 2017). These concentrations pose a potential hazard to organisms. Immunosuppression, nephrotoxicity, and endocrine disruption are some deleterious effects on fishes and mussels (Oba *et al.*, 2021).

Many technologies have been applied to remove IBP from water and wastewater, such as electrochemical and photocatalytic degradation (Li *et al.*, 2016), heterogeneous electro-Fenton process (Liu *et al.*, 2018), ozonation (Saeid *et al.*, 2018), and adsorption (Santaeufemia *et al.*, 2018). However, most of these technologies are expensive, require high-tech operations and skilled personnel, and can generate toxic by-products (secondary pollution) or incomplete removal. Among these technologies, adsorption has become a well-established technology to remove different pollutants, including pharmaceutical drugs. The easy availability, low cost or zero cost of some adsorbents, simplicity of design and operation, and ability to treat wastewater with a low or high concentration of pollutants make the adsorption a techno-economically viable solution for eliminating pollutants from aqueous media (Castro *et al.*, 2017).

Recently, the adsorption of IBP onto biological adsorbents has been studied in detail. Pinewood biochar (Essandoh *et al.*, 2015), *Aegle marmelos* shell biochar (Chakraborty *et al.*, 2018a), and activated sugarcane bagasse (Chakraborty *et al.*, 2018b) are some examples. Microbial biomasses have also been used to efficiently remove pollutants from water (Castro *et al.*, 2017). Their pollutant-adsorptive capacity is due to the chemical characteristics of their cell walls, which possess many polysaccharides and some proteins, among other components. These biomacromolecules have several functional groups, such as carboxyl, amino, thiol, phosphate, and sulfhydryl, responsible for the adsorption phenomena (Ramanaiah *et al.*, 2007).

The yeast *Saccharomyces cerevisiae* is an inexpensive and readily available biomass source used in pollutant adsorption. It can be easily cultivated on a large scale or obtained as a by-product of the food and beverage industries. *Saccharomyces cerevisiae* biomass has been used as a biosorbent to remove heavy metals and textile dyes (Castro *et al.*, 2017). However, this yeast is little-explored with regard to its ability to remove anti-inflammatory drugs. In this study, we investigated the adsorption of IBP by chemically activated *Saccharomyces cerevisiae* biomass under different experimental conditions.

2. MATERIAL AND METHODS

2.1. Chemicals

Ibuprofen sodium salt (IBP) (linear formula: $C_{13}H_{17}O_2Na$; molecular weight: 228.26 g/mol) was obtained from Sigma Aldrich – Brazil (>98% purity, $pK_a = 4.91$). Hexane, methanol, HCl, and NaOH were of analytical grade.

2.2. Preparation and characterization of biosorbent

Saccharomyces cerevisiae was purchased from a local market as Baker's yeast. Yeast biomass (YB) was sieved through a 149 μm standard sieve and activated by extraction with hexane for 6 h and subsequently with methanol for 6 h. The extraction occurred in a Soxhlet extractor. Following the process, the chemically activated yeast biomass (CA-YB) was rinsed with distilled water and dried in an oven at 60°C for 48 h. The CA-YB was kept in a desiccator until use.

2.3. Biosorbent characterization

The functional groups on the surface of CA-YB were investigated using the Fourier transform infrared spectroscopy (FTIR) analyses. The samples of CA-YB were prepared using the KBr disk method, and the transmission FTIR spectra were recorded in the 4000 and 400 cm^{-1} (Shimadzu IRAffinity-1 spectrophotometer). The thermal stability of CA-YB was evaluated with thermogravimetric analysis (TGA) and differential thermal analysis (DTA) using a thermogravimetric analyzer (Shimadzu DTG-60H). The analysis was conducted in an air atmosphere at a heating speed of 20°C/min from ambient temperature (26°C) up to 1000°C. The point of zero charge (pH_{PZC}) of CA-YB was determined using the method described by Dahri *et al.* (2014). 20 mL of KNO_3 solutions (0.1 M) was added to the Erlenmeyer flasks, and the pH values were adjusted in the range of 2.1–10.3 by adding 0.1 M of NaOH/HCl. Then, 0.03 g of CA-YB was added to the Erlenmeyer flasks and the flasks were shaken at 150 rpm for 24 h, at 24°C. Next, the final pH of KNO_3 solutions was measured, and the pH_{PZC} was determined by plotting ΔpH (final pH – initial pH) versus initial pH.

2.4. Batch biosorption experiments

All biosorption experiments were performed with 100 mL Erlenmeyer flasks containing 30 mL of IBP aqueous solution. The flasks were agitated on a shaking incubator at 150 rpm. The influence of various parameters on the biosorption efficiency was evaluated: pH (2, 4, 6, 8, and 10, adjusted by the addition of 0.1 M NaOH or 0.1 M HCl solutions), initial IBP concentration (5.0–35.0 $mg L^{-1}$), contact time (0–90 min), and temperature (20, 30, and 40°C). Aliquots were withdrawn from the flasks at predetermined time intervals and filtered (filter membrane \varnothing 0.45 μm) to remove biosorbent particles. The residual IBP concentration in the solution was analyzed by using a UV/Vis spectrophotometer (Hach DR6000) at $\lambda_{max} = 221$ nm. All biosorption experiments were conducted in triplicate. The IBP removal percentage, R (%), and the amount of IBP adsorbed per unit of biosorbent, q_e ($mg g^{-1}$) were determined according to Equations 1 and 2:

$$R(\%) = \frac{C_i - C_e}{C_i} \times 100 \quad (1)$$

$$q_e = \frac{(C_i - C_e)}{b} \quad (2)$$

Where C_i and C_e are the initial and the equilibrium IBP concentrations (mg L^{-1}), and b is the biosorbent concentration in solution (g L^{-1}).

2.5. Kinetic and isotherms models

The kinetic and isotherms models (Chakraborty *et al.*, 2018b; Santaefemia *et al.*, 2018) used in this study are listed in Table 1. The usability of these models in fitting to data was evaluated by the coefficient of determination (R^2) and the root mean square error (*RMSE*) (Equation 3):

$$RMSE = \sqrt{\frac{1}{n} \sum (q_{exp} - q_{cal})^2} \quad (3)$$

Where q_{exp} and q_{cal} are the experimental and calculated values, and n is the number of samples.

Table 1. Kinetic and isotherm models.

Model	Equation	Parameters
<i>Kinetic models</i>		
Pseudo-first-order	$\log(q_e - q_t) = \log q_e - \frac{K_1}{2.303} t$	q_e (mg g^{-1}): biosorption capacity at equilibrium q_t (mg g^{-1}): biosorption capacity at time t K_1 (min^{-1}): pseudo-first-order rate constant
Pseudo-second-order	$\frac{t}{q_t} = \frac{1}{K_2 q_e^2} + \frac{1}{q_e} t$	K_2 ($\text{g mg}^{-1} \text{min}^{-1}$): pseudo-second-order rate constant
<i>Isotherm models</i>		
Langmuir	$\frac{1}{q_e} = \frac{1}{q_m} + \left(\frac{1}{q_m K_L}\right) \frac{1}{C_e}$	q_e (mg g^{-1}): biosorption capacity at equilibrium q_m (mg g^{-1}): maximum biosorption capacity C_e (mg L^{-1}): equilibrium adsorbate concentration in solution K_L (L mg^{-1}): Langmuir constant
Freundlich	$\ln q_e = \ln K_f + \frac{1}{n} \ln C_e$	K_f ($(\text{mg g}^{-1}) (\text{mg L}^{-1})^{-1/n}$): Freundlich constant n : heterogeneity factor
Dubinin-Radushkevich	$\ln q_e = \ln q_m - \beta \varepsilon^2$	ε : Polanyi potential β ($\text{mol}^2 \text{kJ}^{-2}$): biosorption energy constant
	$\varepsilon = RT \ln \left(1 + \frac{1}{C_e}\right)$	R : universal gas constant ($8.314 \text{ J mol}^{-1} \text{ K}^{-1}$)

2.6. Adsorption thermodynamics

The thermodynamics parameters of IBP biosorption onto CA-YB, *i.e.*, Gibbs free energy change (ΔG), entropy (ΔS), and enthalpy (ΔH), were calculated by using the Equations 4, 5 and 6:

$$\Delta G = -RT \ln K_D \quad (4)$$

$$\Delta G = \Delta H - T\Delta S \quad (5)$$

$$\ln K_D = \frac{\Delta S}{R} - \frac{\Delta H}{R} \times \frac{1}{T} \quad (6)$$

Where K_D (qe/Ce) refers to the distribution coefficient, R is the universal gas constant ($8.314 \text{ J K}^{-1} \text{ mol}^{-1}$), and T (K) is the absolute temperature.

3. RESULTS AND DISCUSSION

3.1. FTIR, TGA-DTA analysis, and pH_{PZC}

FTIR spectroscopy identifies the functional groups on the adsorbents surfaces and the possible interactions between them and the adsorbate. FTIR spectra (Figure 1a) show a diversity of organic compounds on the surface of the pristine cell. The broadband observed in the region $3800\text{--}3000 \text{ cm}^{-1}$ could be assigned to O–H stretching in carbohydrates and N–H stretching of proteins, and amide II of chitin. The peak at 2931 cm^{-1} can be attributed to the CH_2 group of lipids. The peak at 1651 cm^{-1} was assigned to the C=O stretching vibration or N–H bending vibration to the amide I from protein. Bonds of amide II and III (N–H or C–N vibration) also from proteins are observed at peaks 1543 and 1242 cm^{-1} , respectively. The band at 1404 cm^{-1} was due to the symmetric stretching of $-\text{COOH}$, and the peak at 1049 cm^{-1} was C–O stretching vibration of polysaccharides skeleton. The characteristic peak at 578 cm^{-1} corresponds to O–P–O bending vibration of phosphate groups (Chen *et al.*, 2020; Rossi *et al.*, 2020; Wang *et al.*, 2017; Zhang *et al.*, 2019). After the chemical activation of *S. cerevisiae* biomass, the peaks at 3309 (O–H/N–H), 1543 (N–H/C–N), 1049 (C–O), and 578 (O–P–O) cm^{-1} shifted to 3286 , 1535 , 1056 , and 570 cm^{-1} , respectively. After IBP adsorption, some of the bands have shifted from 3286 to 3278 cm^{-1} (O–H/ N–H), 1651 to 1658 cm^{-1} (amide I), 1242 to 1234 cm^{-1} (amide III), 1056 to 1049 (C–O), and 570 o 555 cm^{-1} (O–P–O). These results indicate that the carboxyl, hydroxyl, phosphoryl, and amino groups were involved in the biosorption process of IBP.

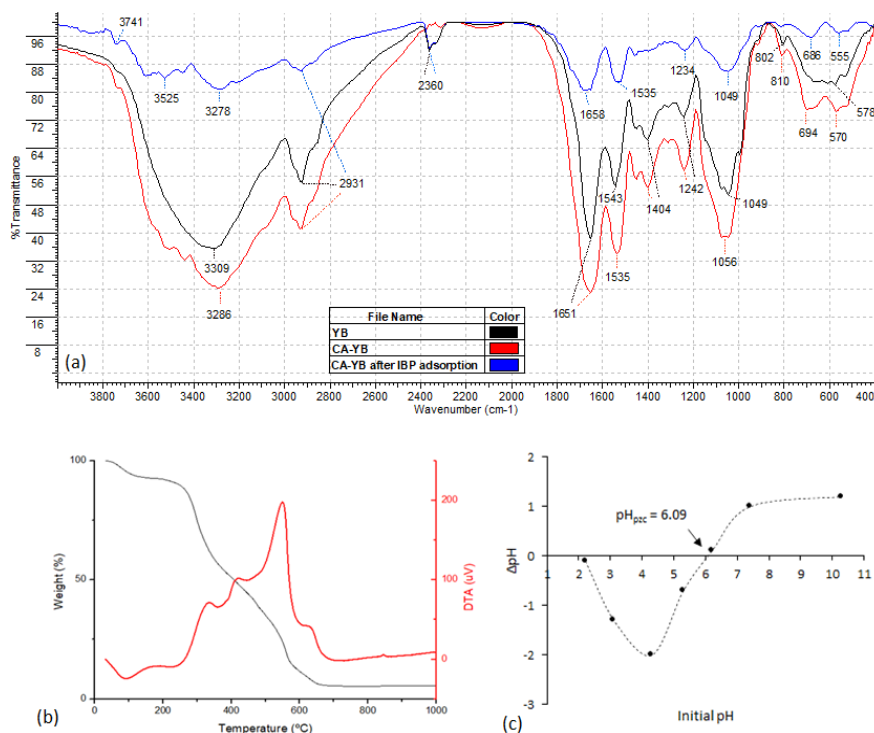


Figure 1. Characterization of CA-YB: FTIR spectra (a), TGA/DTA curve (b), and point of zero charge (pH_{PZC}) (c).

The thermogravimetric diagrams from TGA/DTA are displayed in Figure 1b. The TGA curve from CA-YB decomposition revealed some mass loss steps, which have been accompanied by endothermic and exothermic peaks in the DTA curve. The mass loss observed from room temperature to approximately 130°C is endothermic and corresponds to surface water evaporation. From 130 to 280°C represents the removal region of bound moisture and light volatile compounds (Padmavathy *et al.*, 2003). The maximum mass loss was achieved in the next two exothermic steps, i.e., between 270 and 420°C and 420 and 670°C, indicating that the yeast compounds degraded in these ranges (Rossi *et al.*, 2020). At a temperature above 670°C, no other thermal effects and mass loss were observed.

The point of zero charge (pH_{pzc}) is the pH value where the net charge on the adsorbent surface is zero. The adsorbent surface will be negatively charged when the $\text{pH}_{\text{pzc}} < \text{pH}$ of the solution and positively charged when the $\text{pH}_{\text{pzc}} > \text{pH}$ of the solution. The plot of ΔpH versus initial pH showed that the pH_{pzc} for CA-YB was 6.09 (Figure 1c).

3.2. Effect of pH

The effect of different initial pH on the removal of IBP by CA-YB is shown in Figure 2. The results indicated that the adsorption of IBP decreased from 4.0 to 0.3 mg g⁻¹ when the pH increased from 2 to 10. The removal of IBP by pristine YB was also studied, but the removal was practically negligible (data not shown). The pKa value of ibuprofen is 4.9 (Chakraborty *et al.*, 2018a), and can be used to explain the effect of pH on the IBP biosorption. When the pH value is above 4.9, the anionic form of IBP is the predominant species, while below this value, its molecular form is predominant (Chakraborty *et al.* 2018b). With an increase in the pH, the CA-YB surface becomes less positive, and the anionic form of IBP increases, decreasing the adsorption. At pH 2, the increased IBP removal suggests a minor electrostatic repulsion between the CA-YB surface with IBP.

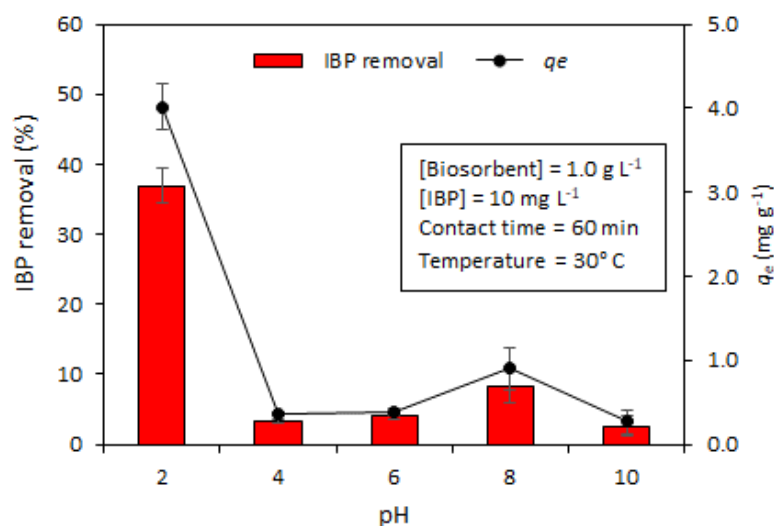


Figure 2. Effect of pH on the biosorption of IBP onto CA-YB.

3.3. Effect of contact time and temperature

Figure 3a shows the IBP biosorption by CA-YB at different contact times and temperatures. Rapid adsorption of IBP occurred during the first 10 min and was practically negligible after this time, which is advantageous considering the practical application. This rapid adsorption is attributed to the abundant availability of free active sites on the biosorbent surface at the beginning of the biosorption process, which became less efficient when these functional groups were occupied. Also, it can be seen that the biosorption capacity of CA-YB increased from 5.37 to 7.29 mg g⁻¹ when the temperature was increased from 20 to 40°C,

indicating that an endothermic process controls the biosorption of IBP onto CA-YB. Since the highest removal efficiency (72,9%) was observed at 40°C, this temperature was used in subsequent experiments.

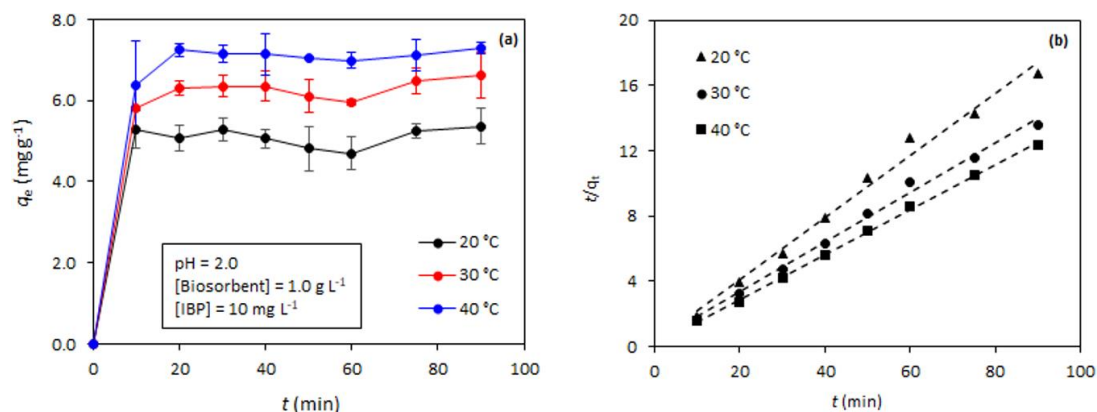


Figure 3. Effect of contact time (a) and plot for pseudo-second-order model (b) for IBP biosorption onto CA-YB, at different temperatures.

3.4. Kinetic studies

Kinetics studies are essential for the modeling and design of the adsorption process. In this study, kinetic experiments of IBP removal were conducted at constant initial IBP concentration (10.0 mg L⁻¹), 1.0 g L⁻¹ of biosorbent, and temperatures of 20, 30, and 40°C. The experimental data of IBP adsorption were fitted with two well-established kinetic models, pseudo-first-order model and pseudo-second-order model (Table 1).

The kinetic parameters (R^2 and $RMSE$) calculated from two kinetic models are summarized in Table 2. Extremely high R^2 values ($R^2 = 0.989-0.99$, Figure 3b) for the pseudo-second-order model for all tested temperatures and values of calculated q_e in agreement with the experimental q_e values indicated that this model was the optimum kinetic model to represent IBP biosorption on CA-YB.

Table 2. Pseudo-first-order and pseudo-second-order kinetic parameters for the biosorption of IBP onto CA-YB, at different temperatures.

Model	Temperature (°C)		
	20	30	40
$q_{\text{experimental}}$	5.37	6.61	7.29
Pseudo-first-order			
q_1 (mg g ⁻¹)	7.43	1.354	4.74
k_1 (min ⁻¹)	0.013	0.016	0.002
R^2	0.121	0.313	0.002
$RMSE$	0.379	0.257	0.436
Pseudo-second-order			
q_2 (mg g ⁻¹)	5.25	6.60	7.26
k_2 (g mg ⁻¹ min ⁻¹)	0.128	0.069	0.142
R^2	0.989	0.994	0.999
$RMSE$	0.600	0.346	0.133

3.5. Equilibrium isotherms

This study conducted equilibrium experiments using solutions with different initial IBP concentrations (5.0-35.0 mg L⁻¹), 1.0 g L⁻¹ of biosorbent at 40°C. The biosorption of IBP onto

CA-YB was evaluated by Langmuir, Freundlich, and Dubinin-Radushkevich (D-R) isotherms models. Figure 4 shows the linearized plots for the isotherm models, and the calculated parameters are presented in Table 3.

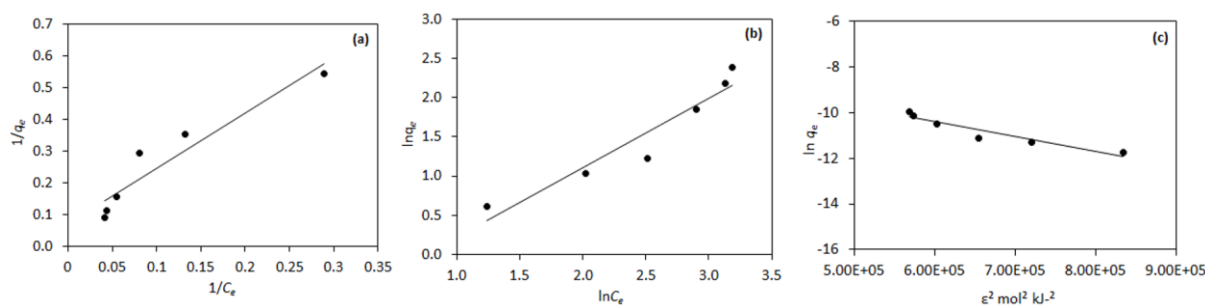


Figure 4. Plots for the isotherm models: (a) Langmuir, (b) Freundlich, and (c) D-R.

Table 3. Isotherm parameters for the biosorption of IBP onto CA-YB.

Model	Parameter
Langmuir	
q_{\max} (mg g ⁻¹)	13.39
K_L (L mg ⁻¹)	0.043
R^2	0.903
$RMSE$	0.049
Freundlich	
K_F (mg g ⁻¹) (mg L ⁻¹) ^{-1/n}	1.940
n	1.133
R^2	0.911
$RMSE$	0.190
D-R	
q_m (mmol g ⁻¹)	1,392
β (mol ² J ⁻²)	6.00 x 10 ⁻⁸
E (kJ mol ⁻¹)	9.129
R^2	0.896
$RMSE$	0.334

Langmuir and Freundlich models described the equilibrium data quite well, with R^2 higher than 0.9 and low $RMSE$. The Freundlich model, however, provided a better R^2 value, with $n > 1.0$, indicating that the biosorption process is favorable (Khadir *et al.*, 2020). The maximum biosorption capacity predicted by the Langmuir model was 13.39 mg g⁻¹. Table 4 compared the maximum adsorption capacities of CA-YB and other adsorbents. It was observed that the IBP adsorption capability using the CA-YB was comparable to those obtained for other adsorbents.

The D-R isotherm model was used to determine the nature of the biosorption process as physical or chemical. From the activity coefficient β , the mean free energy of biosorption (E , kJ mol⁻¹) was estimated using the Equation 7:

$$E = \frac{1}{\sqrt{2\beta}} \quad (7)$$

The biosorption process is controlled by a chemical mechanism when E value falls in the range from 8-16 kJ mol⁻¹, or the biosorption process proceeds through a physical mechanism if $E < 8$ kJ mol⁻¹. The E value of 9.129 kJ mol⁻¹ (Table 3) indicated that the biosorption of IBP onto CA-YB follows a chemical process.

Table 4. Maximum biosorption capacity of IBP onto CA-YB and other adsorbents.

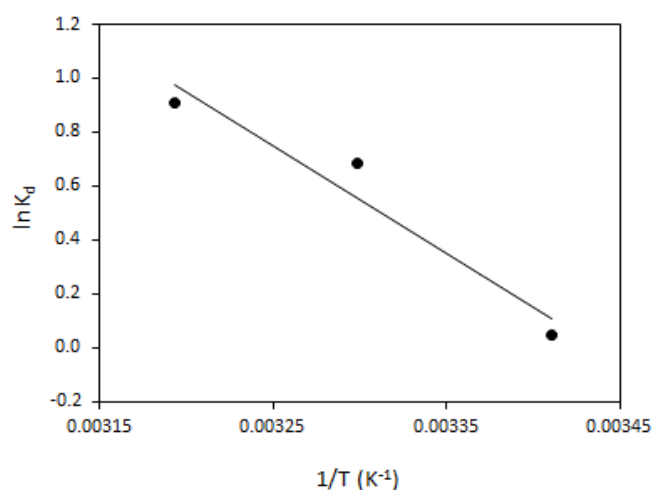
Adsorbent	q_{max} (mg g ⁻¹)
Graphene oxide nanoplatelets (Banerjee <i>et al.</i> , 2016)	3.72
Pine wood biochar (Essandoh <i>et al.</i> , 2015)	10.74
Physically activated <i>Cocos nucifera</i> shell biochar (Chakraborty <i>et al.</i> , 2019)	9.43
Chemically activated <i>Cocos nucifera</i> shell biochar (Chakraborty <i>et al.</i> , 2019)	11.38
Chemically activated date seed biochar (Chakraborty <i>et al.</i> , 2020)	11.23
Steam activated date seed biochar (Chakraborty <i>et al.</i> , 2020)	13.17
Cellulosic Sisal modified by polypyrrole-polyaniline nanoparticles (Khadir <i>et al.</i> , 2020)	19.45
Chemically activated <i>Saccharomyces cerevisiae</i> biomass (Present study)	13.39

3.6. Thermodynamics studies

Values of ΔS and ΔH were calculated by plotting $\ln K_D$ vs $1/T$ (Figure 5). Thermodynamic parameters calculated at different temperatures (20, 30, and 40°C) are summarized in Table 5. The negative values of ΔG indicate that the IBP biosorption onto CA-YB is thermodynamically spontaneous and feasible. The positive ΔH value of 33.07 KJ mol⁻¹ suggests an endothermic biosorption process facilitated by increasing temperature. The ΔS was also found to be positive (113.71 J mol⁻¹ K⁻¹), revealing the affinity of the CA-YB for IBP and showing that the randomness at the solid/solution interface increases during the biosorption of the drug.

Table 5. Thermodynamic parameters estimated for IBP biosorption onto CA-YB.

T (°C)	K_D	ΔG (KJ mol ⁻¹)	ΔH (KJ mol ⁻¹)	ΔS (J mol ⁻¹ K ⁻¹)
20	1.05	-0.263	33.07	113.71
30	1.98	-1.400		
40	2.48	-2.537		

**Figure 5.** Plot of $\ln K_D$ versus $1/T$ for estimation of thermodynamic parameters.

4. CONCLUSIONS

In this study, chemically activated *Saccharomyces cerevisiae* was used for IBP removal from aqueous solution. The highest biosorption rate was found at pH 2. The pseudo-second-order model explained the kinetic data, and both Langmuir and Freundlich isotherm models described the equilibrium data well. The maximum biosorption capacity was estimated at 13.39

mg g⁻¹ at 40°C. The biosorption of IBP onto CA-YB was chemical, endothermic, and spontaneous. FTIR analyses indicated that the carboxyl, hydroxyl, phosphoryl, and amino groups mediated the biosorption process of IBP. These findings proved that CA-YB could be used in IBP biosorption from aqueous media.

5. ACKNOWLEDGMENT

This study was financed in part by the Coordenação de Aperfeiçoamento de Pessoal de Nível Superior – Brasil (CAPES) – Finance Code 001

6. REFERENCES

- ARISTIZABAL-CIRO, C.; BOTERO-COY, A. M.; LÓPEZ, F. J.; PEÑUELA, G. A. Monitoring pharmaceuticals and personal care products in reservoir water used for drinking water supply. **Environmental Science and Pollution Research**, n. 52, p. 7335–7347, 2017. <https://doi.org/10.1007/s11356-016-8253-1>
- BANERJEE, P.; DAS, P.; ZAMAN, A.; DAS, P. Application of graphene oxide nanoplatelets for adsorption of Ibuprofen from aqueous solutions: Evaluation of process kinetics and thermodynamics. **Process Safety and Environmental Protection**, v. 101, p. 45–53, 2016. <https://dx.doi.org/10.1016/j.psep.2016.01.021>
- CASTRO, K. C.; COSSOLIN, A. S.; REIS, H. C. O.; MORAIS, E. B. Biosorption of anionic textile dyes from aqueous solution by yeast slurry from brewery. **Brazilian Archives of Biology and Technology**, v. 60, p. 1-13, 2017. <http://dx.doi.org/10.1590/1678-4324-2017160101>
- CHAKRABORTY, P.; BANERJEE S.; KUMAR, S.; SADHUKHAN, S.; HALDER, G. Elucidation of ibuprofen uptake capability of raw and steam activated biochar of *Aegle marmelos* shell: Isotherm, kinetics, thermodynamics and cost estimation. **Process Safety and Environmental Protection**, v. 118, p. 10–23, 2018a. <https://doi.org/10.1016/j.psep.2018.06.015>
- CHAKRABORTY, P.; SHOW, S.; BANERJEE, S.; HALDER, G. Mechanistic insight into sorptive elimination of ibuprofen employing bi-directional activated biochar from sugarcane bagasse: Performance evaluation and cost estimation. **Journal of Environmental Chemical Engineering**, v. 6, n. 4, p. 5287–5300, 2018b. <https://doi.org/10.1016/j.jece.2018.08.017>
- CHAKRABORTY, P.; SHOW, S.; RAHMAN, W. U.; HALDER, G. Linearity and non-linearity analysis of isotherms and kinetics for ibuprofen remotion using superheated steam and acid modified biochar. **Process Safety and Environmental Protection**, v. 126, p. 193–204, 2019. <https://doi.org/10.1016/j.psep.2019.04.011>
- CHAKRABORTY, P.; SINGH, S. D.; GORAI, I.; SINGH, D.; RAHMANA, W. U.; HALDER, G. Explication of physically and chemically treated date stone biochar for sorptive remotion of ibuprofen from aqueous solution. **Journal of Water Process Engineering**, v. 33, p. 1-11, 2020. <https://dx.doi.org/10.1016/j.jwpe.2019.101022>
- CHEN, C.; HU, J.; WANG, J. Biosorption of uranium by immobilized *Saccharomyces cerevisiae*. **Journal of Environmental Radioactivity**, v. 213, p. 1-10, 2020. <https://doi.org/10.1016/j.jenvrad.2020.106158>

- DAHRI, M. K.; KOOH, M. R. R.; LIM, L. B. L. Water remediation using low cost adsorbent walnut shell for removal of malachite green: Equilibrium, kinetics, thermodynamic and regeneration studies. **Journal of Environmental Chemical Engineering**, v. 2, n. 3, p. 1434–1444, 2014. <https://doi.org/10.1016/j.jece.2014.07.008>
- ESSANDOH, M.; KUNWAR, B.; PITTMAN, C. U.; MOHAN, D.; MLSNA, T. Sorptive removal of salicylic acid and ibuprofen from aqueous solutions using pine wood fast pyrolysis biochar. **Chemical Engineering Journal**, v. 265, p. 219–227, 2015. <https://doi.org/10.1016/j.cej.2014.12.006>
- KHADIR, A.; MOTAMEDI, M.; NEGARESTANI, M.; SILLANPÄÄ, M.; SASANI, M. Preparation of a nano bio-composite based on cellulosic biomass and conducting polymeric nanoparticles for ibuprofen removal: Kinetics, isotherms, and energy site distribution. **International Journal of Biological Macromolecules**, v. 162, p. 663–677, 2020. <https://doi.org/10.1016/j.ijbiomac.2020.06.095>
- LI, F.; KANG, Y.; CHEN, M.; LIU, G.; LV, W.; YAO, K.; CHEN, P.; HUANG, H. Photocatalytic degradation and removal mechanism of ibuprofen via monoclinic BiVO₄ under simulated solar light. **Chemosphere**, v. 150, p. 139–144, 2016. <https://doi.org/10.1016/j.chemosphere.2016.02.045>
- LIU, D.; ZHANG, H.; WEI, Y.; LIU, B.; LIN, Y.; LI, G. *et al.* Enhanced degradation of ibuprofen by heterogeneous electro-Fenton at circumneutral pH. **Chemosphere**, v. 209, p. 998–1006, 2018. <https://doi.org/10.1016/j.chemosphere.2018.06.164>
- OBA, S. N.; IGHALO, J. O.; ANIAGOR, C. O.; IGWEGBE, C. A. Removal of ibuprofen from aqueous media by adsorption: A comprehensive review. **Science of The Total Environment**, v. 780, p. 1-23, 2021. <https://doi.org/10.1016/j.scitotenv.2021.146608>
- PADMAVATHY, V.; VASUDEVAN, P.; DHINGRA, S. C. Thermal and spectroscopic studies on sorption of nickel (II) ion on protonated baker's yeast. **Chemosphere**, v. 52, p. 1807–1817, 2003. [https://doi.org/10.1016/S0045-6535\(03\)00222-4](https://doi.org/10.1016/S0045-6535(03)00222-4)
- RAMANAIAH, S. V.; VENKATA MOHAN, S.; SARMA, P. N. Adsorptive removal of fluoride from aqueous phase using waste fungus (*Pleurotus ostreatus* 1804) biosorbent: Kinetics evaluation. **Ecological Engineering**, v. 31, n. 1, p. 47–56, 2007. <https://doi.org/10.1016/j.ecoleng.2007.05.006>
- ROSSI, A.; RIGUETO, C. V. T.; DETTMER, A.; COLLA, L. M.; PICCIN, J. S. Synthesis, characterization, and application of *Saccharomyces cerevisiae*/alginate composites beads for adsorption of heavy metals. **Journal of Environmental Chemical Engineering**, v. 8, n. 4, p. 1-7, 2020. <https://doi.org/10.1016/j.jece.2020.104009>
- SAEID, S.; TOLVANEM, P.; KUMAR, N.; ERÄNEN, K.; PELTONEN, J.; PEURLA, M. *et al.* Advanced oxidation process for the removal of ibuprofen from aqueous solution: A non-catalytic and catalytic ozonation study in a semi-batch reactor. **Applied Catalysis B: Environmental**, v. 230, p. 77–90, 2018. <https://doi.org/10.1016/j.apcatb.2018.02.021>
- SANTAEUFEMIA, S.; TORRES, E.; ABALDE, J. Biosorption of ibuprofen from aqueous solution using living and dead biomass of the microalga *Phaeodactylum tricornutum*. **Journal of Applied Phycology**, v. 30, n. 1, p. 471–482, 2018. <https://doi.org/10.1007/s10811-017-1273-5>

- WANG, T.; ZHENG, X.; WANG, X.; LU, X.; SHEN, Y. Different biosorption mechanisms of Uranium (VI) by live and heat-killed *Saccharomyces cerevisiae* under environmentally relevant conditions. **Journal of Environmental Radioactivity**, v. 167, p. 92–99, 2017. <https://doi.org/10.1016/j.jenvrad.2016.11.018>
- YAMKELANI, N.; NCUBE, N.; MAHLAMBI, P. N.; CHIMUKA, L.; MADIKIZELA, L. M. Adsorbents and removal strategies of non-steroidal anti-inflammatory drugs from contaminated water bodies. **Journal of Environmental Chemical Engineering**, v. 7, n. 3, p. 1-14, 2019. <https://doi.org/10.1016/j.jece.2019.103142>
- ZHANG, J.; CHEN, X.; ZHOU, J.; LUO, X. Uranium biosorption mechanism model of protonated *Saccharomyces cerevisiae*. **Journal of Hazardous Materials**, v. 385, p. 1-10, 2019. <https://doi.org/10.1016/j.jhazmat.2019.121588>